

Forschungsschwerpunkt S92

# Industrial Geometry

<http://www.ig.jku.at>



FSP Report No. 41

## Combined evolution of level sets and B-spline curves for imaging

M. Fuchs, B. Jüttler, O. Scherzer and H.  
Yang

January 2007

**FWF**

Der Wissenschaftsfonds.



**Abstract** We propose the evolution of curves in direction of their unit normal using a combined implicit and explicit spline representation according to a given velocity field. In the implicit case we evolve a level set function for segmentation and geometry reconstruction in 2D images. The level set approach allows for topological changes of the evolving curves. The evolution of the explicit B-spline curve is driven by the Mumford-Shah functional.

We are mainly concerned with the segmentation of images using active contours. To get satisfactory results from the implicit evolution the optimal stopping time and the correct level of the evolving function has to be estimated. We overcome this problem by using the combined evolution.

As a second application we focus at controlling the topology of the level set function used to detect geometries via EIT. The concurrent evolution of spline curves enables us to identify geometries of dimension 1 which would be lost using only the level set approach.

M. Fuchs · B. Jüttler · O. Scherzer · H. Yang

# Combined evolution of level sets and B-spline curves for imaging

the date of receipt and acceptance should be inserted later

---

## 1 Introduction

Level set methods introduced in [21] are widely used in imaging to reconstruct geometries [6, 7, 9, 11, 10, 12]. They automatically handle complex topologies, i.e. we can detect and represent objects consisting of different components by only one level set function. Also multiply connected sets can be reconstructed. On the other hand, since the geometry is implicitly hidden in the graph of the level set function, one does not have direct control over the geometry represented by the zero level set. The additional evolution of curves driven by the speed function adds the advantages of an explicit representation to those of the level set evolution. We focus on the application of this approach to the segmentation of 2D gray-scale images. Secondly we suggest a way to use the additional information provided by the spline evolution to handle the correct detection of perfectly insulating cracks in the EIT problem.

### 1.1 Image Segmentation

Several approaches to image segmentation have been developed. One of them is the reconstruction of the boundary of an object by detecting closed curves of high gradients in the image. This is for instance described in [15]. There the authors propose to minimize an energy functional with respect to admissible splines such that the minimizing splines optimally adapt to edges in the

image, i.e. 1-dimensional features with high image gradients.

One possibility to obtain such a minimizer is to evolve a closed curve from either outside or inside an object towards the object boundaries. The speed of the evolution is determined by the image gradients and should be zero at the boundary. In this approach of active contours the following issues have to be taken care of:

- In regions, where no high image gradients occur, the speed of the evolution has to be kept above a certain level to provide convergence of the method. Noise in the image, should *not* stop the evolution.
- The evolution *should* stop at the boundaries of the object. The difficulty here is to correctly identify an image region of high variation as a boundary. As mentioned before, image noise can result in locally high gradients. Thus, the shape of the moving contour in the region in question has to be taken into account as well as the absolute value of the gradient. In other words, the evolving curve should not get stuck at unwanted artifacts but, on the other side, must not cross the object boundary.
- The regularity of the active contour has to be maintained. If we require the curvature of the contour to be bounded, it cannot stop at arbitrarily small artifacts anymore. Secondly, even if we were able to capture the exact boundary of an object, it may be desired to further smooth the contour.
- Also the actual representation of the active contour is of interest. In level set implementations the curve will be the zero level set of a function discretized at pixel level. For applications it can be crucial to have a spline representation of the contour at hand, which allows for easy corrections and adaptations in a manual post-processing step. Secondly information about the actual shape of the segmented object can be acquired from a parametric representation more easily. A simple example is the number of components of the segmentation which is directly accessi-

---

M. Fuchs and O. Scherzer  
Leopold-Franzens-Universität, Department of Computer Science, Innsbruck, Austria  
E-mail: matz.fuchs@uibk.ac.at  
E-mail: otmar.scherzer@uibk.ac.at

B. Jüttler and H. Yang  
Johannes-Kepler-Universität, Institute of Applied Geometry, Linz, Austria,  
E-mail: bert.juettler@jku.at  
E-mail: yang.huaiping@jku.at

ble by simply counting the number of evolving spline curves.

A level set implementation of active contours was proposed in [6] and extended in [7]. In the latter paper the authors propose to evolve a level set function on  $\mathbb{R}^2$  according to

$$\begin{aligned} u(0) &= u^0, \\ \frac{\partial u}{\partial \tau} &= |\nabla u|g(I_\sigma)\left(\nabla \cdot \left(\frac{\nabla u}{|\nabla u|}\right) + \gamma\right) \\ &\quad + \nabla g(I_\sigma) \cdot \nabla u, \end{aligned} \quad (1.1)$$

where  $g : \mathbb{R} \rightarrow \mathbb{R}$  is a the so-called *edge-detector*, i.e. a non-increasing, positive and differentiable function, converging to 0 as its argument tends to infinity. We denote the function defined by  $g(I_\sigma(x)) = g(|\nabla I_\sigma(x)|)$  for  $x \in \mathbb{R}^2$  as  $g(I_\sigma)$ , where  $I_\sigma$  is the image  $I : \mathbb{R}^2 \rightarrow \mathbb{R}$  after convolution with the Gaussian kernel determined by  $\sigma$ . In accordance with [7] we call the parameter  $\gamma > 0$  the *balloon force*. It is added to the curvature of  $u$  in the first term of (1.1). This ensures that the level sets move even in case their curvature is 0.

Assuming sufficient regularity on  $I$  and  $u^0$  the authors prove that a solution in the sense of viscosity solutions of this equation exists. Considering objects with boundaries  $\{x \in \mathbb{R}^2 : g(I)(x) = 0\}$  they further show that all level sets of  $u^0$ , which initially enclose the object, converge to the boundary of the object with respect to the Hausdorff distance.

Because of the level set approach, this evolution automatically adapts to topology changes. There exist numerous implementations of this PDE. In the original paper [7], the authors used finite differences both in time and space. Kühne et al. [17] proposed the so-called *AOS scheme* for efficient implementation. Yang et al. [22] use a T-Spline representation of the level set function. For the results in this paper we discretized the space domain with finite elements and used finite differences in time.

All of the above mentioned implementations share the following parameters:

- The balloon force  $\gamma$ .
- The initial level set function  $u^0$ .
- The edge detector  $g$ . Regardless of the exact function chosen for as edge detector, there will be a parameter  $\eta$  controlling how sensitive the edge detector is with respect to gradients. Common choices for  $g$  are

$$g(t) = \exp(\eta t^2) \quad \text{or} \quad g(t) = \frac{1}{1 + \eta t^2}.$$

Often semi-implicit schemes additionally require to regularize the term  $|\nabla u|$  to avoid singularities. The regularization also influences the results of these methods.

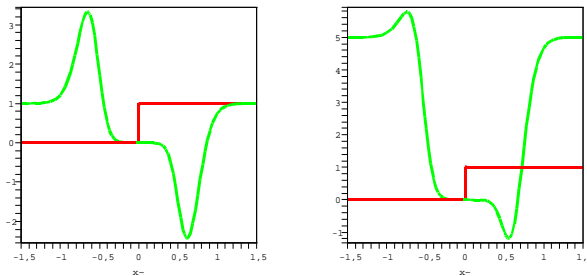


**Fig. 1** Force function (green) for the Heaviside function (red). We chose  $\sigma = .4$  and  $\eta = 10$ . The balloon force is  $\gamma = 1$  (left) and  $\gamma = 5$  (right).

The influence of  $\gamma$  is illustrated by the following example. The explicit evolution of the zero level set of (1.1) is given by

$$\frac{\partial C}{\partial \tau} \cdot \mathbf{n} = g(I_\sigma)(\gamma + \kappa) - (\nabla g(I_\sigma) \cdot \mathbf{n}),$$

where  $C$  denotes the evolving the curve,  $\kappa$  its curvature and  $\mathbf{n}$  its normal. For simplicity we focus on the 1-dimensional case and assume  $\kappa = 0$ . We then see that the explicit curve is driven by the force  $\gamma g(I_\sigma) - |g'(I_\sigma)|$ . Consider the image  $I = H$ , the Heaviside function. In Figure 1 we plotted the attraction force in this case for different parameters  $\gamma$  and  $\eta$ . Imagine the active contour arriving from the left. In the regions where the force function is positive the contour is pushed towards the edge (at 0). The negative force pulls the contour back again and traps it at 0. If the region of negative force is small, it is likely that the curve crosses the edge due to numerical inaccuracies.

When using the above method we often observe that already detected parts of the boundary in the outer regions of the image vanish before the central image regions are segmented. This is illustrated in the upper three images in Figure 2. At no time  $\tau$  the complete boundary of the object is correctly detected, since the active contour crosses the boundary in the outer regions at an early stage of the evolution.

There are two main reasons for this phenomenon. First, the active contour crosses the boundary if the gradient at the edge is too small for the edge detector to locally stop the evolution. This essentially means that the user has to choose a high enough value for  $\eta$  to stop the evolving curve at the “right” edge. In other words, the choice of the parameter  $\eta$  determines the steepness of the edges which will eventually be detected.

Secondly, the first term in the evolution equation never degenerates completely and thus the level set function increases due to the balloon force. Therefore, after some time  $u$  is raised above the zero level and the boundary of the object vanishes.

In Figure 2 the latter effect clearly dominates. Obviously the information on the object boundary is still

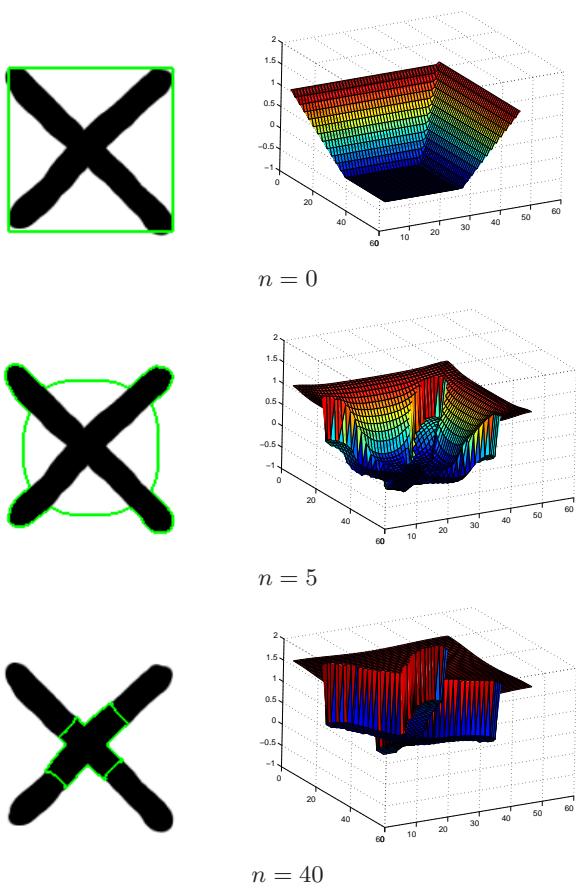


**Fig. 2** Vanishing boundary at the outer regions of the image.

available at any time but can not be captured by the zero level set.

This is visible first at the outer parts of the image domain, where the initial function is close to 0. Note that theoretically the problem does not exist, but it occurs due to technical limitations in the implementation of equation (1.1) and is amplified by large balloon forces  $\gamma$  as it is explained in more detail in the following:

- To ensure that in each time step we solve a PDE in divergence form, we have to divide equation (1.1) by  $|\nabla u|$ . In numerical realizations this term has to be regularized to avoid divisions by zero, i.e. we substitute  $|\nabla u|$  by  $\sqrt{\nabla u \cdot \nabla u + \varepsilon^2}$  for some small  $\varepsilon > 0$ . We call this approximation of the gradient  $\varepsilon$ -regularization. This modification implies that the principal component of the evolution equation is always positive, even if the level set function is flat. To approximate the original equation, it is preferable to choose  $\varepsilon$  as small as possible, but clearly this choice is limited by numerical considerations.
- It is desirable to choose  $\gamma$  large for two reasons. Firstly, higher values of  $\gamma$  give faster evolution speeds. Secondly, Caselles et al. *require*  $\gamma$  to be large enough

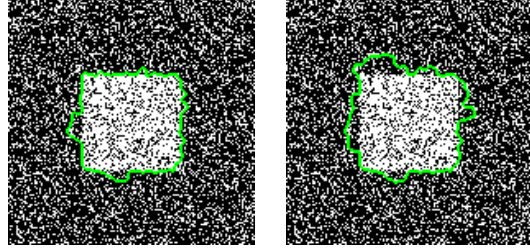


**Fig. 3** Detection of a square with salt & pepper noise added: solution of the evolution at  $\tau = 1800$  started from an initial function  $u^0$  (left) and from  $5u^0$  (right).

to obtain the result concerning consistency of the active contour method in [7].

Unfortunately the influence of the  $\varepsilon$ -regularization is multiplied by the balloon force. Thus, one has to balance evolution speed against the  $\varepsilon$ -regularization.

- A very steep initial function  $u^0$  is robust against the effect of vanishing boundaries. E.g. it is possible to avoid the problems in Figure 2 by rescaling  $u^0$ . The drawback is that steep level set functions are more sensitive to noise. This is illustrated in Figure 3. Again a compromise between sensitivity to noise and global stability of the result has to be found.

All the above issues cause the level lines of the evolving function  $u$  to move across the boundary of the object we want to detect. If this happens, we can not extract a reliable segmentation from the zero level set anymore. Thus, we consider a method to extract the boundary information from the level set function without sticking to a specific level. We propose to evolve a B-Spline curve, which splits according to the topology information provided by the normal vectors of the level set function. By combining the evolution of the active contour with a Mumford-Shah type segmentation of the level set function we inherently use the information of *all* level sets in contrast to tracking only one. We go even further by additionally using the derivative of the level set function to extract information about the topology of the target shape. The B-Spline representation can easily be manually adapted during or after the evolution and allows for precise control of the regularity of the resulting contour.

## 1.2 Electrical Impedance Tomography

Electrical Impedance Tomography (EIT) is concerned with the identification of inclusions in a conductor by measuring the potentials induced by current fluxes on the boundary. Assuming a planar conductor (i.e. the 2-dimensional case) and the special case of perfectly isolating inclusions and constant conductivity on the remaining region, it can be shown [14, 2, 16] that the inclusions can be uniquely determined by at most two

measurements. This result holds for inclusions of dimension 2 and 1.

The actual identification of these inclusions by computational means is an ill-posed inverse problem. Results concerning the (in-)stability of the reconstruction can be found in [14, 1, 3, 5, 4]. We will focus on a level set implementation which is similar to [10, 12]. This iterative approach starts with a level set function such that the zero level set corresponds to the initial guess of the inclusion. The level set function evolves according to the minimizing gradient flow of a regularization functional. Thus, we have a level set evolution

$$u^{k+1} = u^k - \delta \nabla F(u^k),$$

where  $F$  is the regularization energy (corresponding to the EIT problem) and  $\nabla F$  its derivative with respect to the level set function  $u$ . Then  $u^k$  is supposed to converge to a function  $\tilde{u}$  in the  $L^2$  sense, such that  $\{x \in \Omega : \tilde{u}(x) \geq 0\}$  is the isolating inclusion we seek.

Now assume that this inclusion is a crack, i.e. a 1-dimensional set. Then, it can not be characterized by a level set function of class  $L^2$  anymore and the above method will fail. In other words, a level set method which is known to detect inclusions in a conductor in the  $L^2$ -sense only, does not work for cracks anymore, because 1-dimensional features will be lost with such a method.

We propose to use a combined evolution in the iterative computation of such level set functions. It might allow us to detect the development of level sets of dimension 1 in advance and to cope with such cases. This approach is very similar to the case of image segmentation and is described in detail in Section 4.

## 2 The combined evolution

As in the introduction we assume a gray-scale image  $I : \mathbb{R}^2 \rightarrow \mathbb{R}$  and an initial level set function  $u^0$ . Let further  $u : [0, \infty[ \times \mathbb{R}^2 \rightarrow \mathbb{R}$  be a solution of (1.1) and  $C_j : [0, 1] \rightarrow \mathbb{R}^2$ ,  $1 \leq j \leq k$ , simple Jordan curves, which do not intersect each other (or lie within each other). By  $\mathcal{J}(C)$  and  $\mathcal{O}(C)$  we denote the regions inside and outside a Jordan curve  $C : [0, 1] \rightarrow \mathbb{R}^2$ . We further define

$$\begin{aligned} \mathcal{J}(C_1, \dots, C_k) &= \bigcup_{1 \leq j \leq k} \mathcal{J}(C_j) \text{ and} \\ \mathcal{O}(C_1, \dots, C_k) &= \bigcap_{1 \leq j \leq k} \mathcal{O}(C_j). \end{aligned}$$

A slightly modified version of the Mumford-Shah functional [19, 20], for  $k$  curves is given by

$$\begin{aligned} I(C_1, \dots, C_k) &= \alpha \int_{\mathcal{J}(C_1, \dots, C_k)} (u_1 - f)^2 dx \\ &+ \alpha \int_{\mathcal{O}(C_1, \dots, C_k)} (u_2 - f)^2 dx \\ &+ \beta \sum_{j=1}^k L_2^2(C_j), \end{aligned} \quad (2.1)$$

where  $\alpha, \beta > 0$  and

$$u_1 = \text{avg} \int_{\mathcal{J}(C_1, \dots, C_k)} f dx \text{ and } u_2 = \text{avg} \int_{\mathcal{O}(C_1, \dots, C_k)} f dx.$$

Here

$$\text{avg} \int_A f dx := \frac{1}{|A|} \int_A f dx$$

is the average of a function  $f$  over a set  $A$ . The functional (2.1) is also used in [11].

We want to minimize the above energy functional by solving the variational problem  $I \rightarrow \min$ . Assume that  $C'_1, \dots, C'_k$  are curves of minimal energy. Then the function

$$u' = u_1 \chi_{\mathcal{J}(C_1, \dots, C_k)} + u_2 \chi_{\mathcal{O}(C_1, \dots, C_k)}$$

is a piecewise constant function, which is discontinuous along the boundaries of  $C_j$  only and approximates  $u$  in the  $L^2$  sense.

Differentiation of  $I(C_1, \dots, C_k)$  with respect to  $C_j$ ,  $1 \leq j \leq k$ , yields the following gradient descent:

$$\frac{\partial C_j}{\partial \tau}(\tau) = -\nabla I(C_j(\tau)), \quad 1 \leq j \leq k, \quad (2.2)$$

where

$$\begin{aligned} -\nabla I(C) &= \alpha \left( (u_2(C) - u \circ C)^2 \right. \\ &\quad \left. - (u_1(C) - u \circ C)^2 \right) |C'| \mathbf{n}_j \\ &+ \beta |C'| C'', \end{aligned} \quad (2.3)$$

for a curve  $C$ . Here  $\nabla I$  is the derivative of the energy functional  $I$  in (2.1) with respect to  $C$ . Although we denote it by  $\nabla I$ , it can not be expressed as a matrix since  $I$  is defined on an infinite-dimensional space.

Note that we include the derivative of  $C$  with respect to the curve parameter  $t$  in  $\nabla I(C)$ . I.e. the directional derivative of the functional  $I$  in  $C$  into the direction  $D$  can be computed by simply integrating  $\nabla I(C) \cdot D$  over the parameter interval  $[0, 1]$ ,

$$DI(C)(D) = \int_0^1 \nabla I(C)(t) \cdot D(t) dt.$$

Assume  $k$  initial curves  $C_1^0, \dots, C_k^0$ . Combining equations (1.1) and (2.3) gives

$$\begin{aligned} u(0) &= u^0, \\ C_j(0) &= C_j^0, \quad 1 \leq j \leq k, \\ \frac{\partial u}{\partial \tau} &= |\nabla u| g(I_\sigma) \left( \nabla \cdot \left( \frac{\nabla u}{|\nabla u|} \right) + \gamma \right) + \nabla g(I_\sigma) \cdot \nabla u, \\ \frac{\partial C_j}{\partial \tau} &= -\nabla I(C_j(\tau)). \end{aligned} \quad (2.4)$$

In the above equation  $u$  and  $C_j$  and hence also  $\mathbf{n}$  and  $\kappa$  are functions of the time  $\tau$ , i.e.  $u = u(\tau)$ ,  $C_j = C_j(\tau)$ ,  $\mathbf{n} = \mathbf{n}(\tau)$  and  $\kappa = \kappa(\tau)$ . Note that this system is decoupled in the sense that the equations governing the evolution of the  $C_j$ ,  $1 \leq j \leq k$  depend on the first equation (the evolution of  $u$ ) but not the other way round.

In the following we motivate the use of this evolution for segmentation. Theorem 1 shows that the level set function of the above evolution converges to the indicator function of the object which is to be detected. It is based on the results in [7]. We will state all of the following results for the case  $k = 1$  to simplify the notation. The generalization to the case  $k > 1$  is straightforward.

**Theorem 1 (Caselles et al.)** *Assume that the edge detector  $g(I_\sigma) : \mathbb{R}^2 \rightarrow [0, \infty[$  satisfies  $g(I_\sigma) \geq 0$  and*

$$\sup_{x \in \mathbb{R}^2} |\nabla g^{1/2}(x)| < \infty \quad \text{and} \quad \sup_{x \in \mathbb{R}^2} |D^2 g(x)| < \infty.$$

*Let further be  $\hat{C} : [0, 1] \rightarrow \mathbb{R}^2$  a simple  $C^2$ -Jordan curve, which parametrizes*

$$\{x \in \mathbb{R}^2 : g(I)(x) = 0\} = \text{image}(\hat{C}),$$

*and is such that  $\nabla g(I) = 0$  on  $\text{image}(\hat{C})$ .*

*We require the initial function  $u^0 : \mathbb{R}^2 \rightarrow \mathbb{R}$ ,  $u^0 \geq 0$ , to be of class  $u^0 \in \mathcal{C}^2(\mathbb{R}^2)$ . Further  $u^0$  should be 1 on a neighborhood of  $\mathcal{J}(\hat{C})$  and 0 outside a bounded set  $\Omega \subseteq \mathbb{R}^2$ .*

*Define for  $0 < h \leq 1$*

$$C(\tau, h) = \partial\{x \in \mathbb{R}^2 : u(\tau, x) \geq h\}.$$

*Then there exists a unique viscosity solution  $u(\tau, x)$  of (1.1) satisfying*

$$\inf_{x \in \mathbb{R}^2} u^0(x) \leq u(\tau, x) \leq \sup_{x \in \mathbb{R}^2} u^0(x) \quad \text{for } \tau \geq 0.$$

*If  $\gamma$  is large enough then the following results hold: For every  $0 < h \leq 1$*

$$\lim_{\tau \rightarrow \infty} C(\tau, h) = \hat{C} \quad (2.5)$$

*with respect to the Hausdorff distance, and*

$$\lim_{\tau \rightarrow \infty} u(\tau) = \chi_{\mathcal{J}(\hat{C})} \quad \text{in the } L^2\text{-sense.} \quad (2.6)$$

*Proof* The result concerning existence and uniqueness and (2.5) has been proved in [7].

Thus, it remains to prove (2.6). In the proof of Theorem 5 in [7] and Theorem 4 in [8] the authors obtain the result (2.5) by showing that for  $\varepsilon > 0$  and  $0 < h \leq 1$  there exists  $\tau^0 > 0$  such that for  $\tau \geq \tau^0$  the level set function is bounded by  $h$  on the outside of the  $\varepsilon$ -offset of  $\hat{C}$ , i.e.

$$\sup \{u(\tau, x) : x \in \mathbb{R}^2, x \notin \mathcal{J}(\hat{C})_\varepsilon, \tau > \tau^0\} < h.$$

Here  $\mathcal{J}(\hat{C})_\varepsilon = \mathcal{J}(\hat{C}) + B_\varepsilon(0)$ . Secondly,  $u(\tau, x) = 0$  on  $\mathbb{R}^2 \setminus \Omega$ .

Now assume  $\varepsilon > 0$  and let  $\tau^0$  be as above for the special case  $h = 1 - \varepsilon$ . Then

$$\begin{aligned} \int_{\mathbb{R}^2} (\chi_{\mathcal{J}(\hat{C})} - u(\tau))^2 dx &\leq \int_{\Omega \setminus \mathcal{J}(\hat{C})_\varepsilon} \varepsilon^2 + \int_{\mathcal{J}(\hat{C})_\varepsilon \setminus \mathcal{J}(\hat{C})} 1 dx \\ &\leq |\Omega| \varepsilon^2 dx + |\hat{C} + B_\varepsilon(0)|, \end{aligned}$$

since  $u(\tau) = 1$  on  $\mathcal{J}(\hat{C})$  for all  $\tau \geq 0$ . Here  $|\cdot|$  denotes the 2-dimensional Lebesgue measure of a set. Note that the above convergence holds also in  $L^p$  for  $1 \leq p < \infty$ .  $\square$

Theorem 1 states that for  $\tau \rightarrow \infty$  the function  $u(\tau)$  converges to the indicator function of the object. It is difficult to prove analytically, but intuitively evident that the curve  $C$  approximates the boundary of the object as well. The parameter  $\alpha$  controls the smoothness of the boundary  $C$  during the evolution. This allows for effective capturing of objects with noisy boundary.

In general the viscosity solution does not have to be differentiable but is just continuous. However, we can still compute the generalized gradient  $\nabla u$  in every point. If  $|\nabla u|$  is finite and positive then  $\frac{\nabla u}{|\nabla u|}$  is the unit normal of the level sets of  $u$ . Thus, in the view of Theorem 1, we can at least formally expect that

$$\frac{\nabla u(\tau)}{|\nabla u(\tau)|} \approx \mathbf{n}(\tau) \quad \text{for } \tau \rightarrow \infty. \quad (2.7)$$

We will use this observation to correctly adapt the topology of the moving spline curves  $C_j$  during the evolution. If during the evolution two separate parts of  $C_j$  get close to each other and the relation (2.7) does not hold in this area, we have to split the curve into two curves. This is illustrated in Figure 4 and explained in more detail in the next section.

### 3 Implementation

To solve (2.4) numerically we model  $u(\tau)$  using bilinear finite elements on a regular pixel-sized grid. The evolving spline curve  $C(\tau)$  is implemented with periodic cubic B-splines.

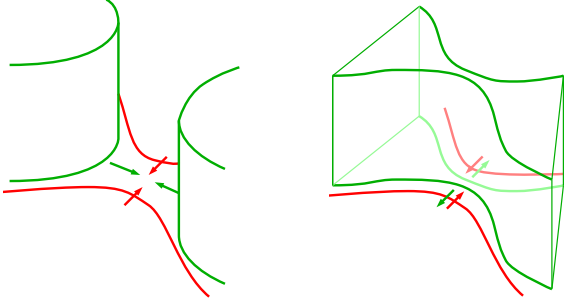


**Fig. 4** Adaptation of the topology of the evolving spline curve (red) to the topology prescribed by the level set function (green). On the left the normals of the spline curve and the gradients of the level set function are orthogonal to each other. This indicates that the spline curve has to be splitted. On the right the two segments of the spline curve are very close to each other but there topology conforms with the level set function. No splitting is performed.

The numerical solution of (2.4) is performed in three steps. At a given time  $\tau \geq 0$  we compute an approximate solution  $u(\tau + \delta)$  by solving the semi-implicit system of equations derived from the FE-formulation. In the second step we evolve  $C(\tau)$  to  $\tau + \delta$  using explicit steps in time. In the last step we detect topology changes by comparing the gradients of the level set function to the curve normals as explained in Figure 4. In case the topology of the curve does not correspond to the level set topology (which we assume to be correct), we adapt the curve to the level-set function by splitting into more components. Finally we proceed with computing the next step of the semi-implicit evolution.

### 3.1 Level set evolution

For  $\tau \geq 0$  and the time step  $\delta > 0$  the semi-implicit time discretization of (1.1) on  $\Omega$  reads as

$$\frac{u(\tau + \delta) - u(\tau)}{\delta} = |\nabla u(t)| \nabla \cdot \left( g(I_\sigma) \frac{\nabla u(t + \tau)}{|\nabla u(t)|} \right) + \gamma |\nabla u(t + \tau)| g(I_\sigma).$$

We cover the rectangular image domain  $\Omega$  with square elements with corners at the centers of the image pixels. On this grid we define bilinear basis functions  $(\varphi^n)_{1 \leq n \leq N}$ . Then we identify

$$u^0(x) = \sum_{n=1}^N u_n^0 \varphi^n(x) \text{ and} \\ u(\tau, x) = \sum_{n=1}^N u_n(\tau) \varphi^n(x) \text{ for } x \in \Omega.$$

Multiplying the above equation by a test function  $\varphi^m$ ,  $1 \leq m \leq N$ , and inserting the base function representa-

tion of  $u$  and integrating it over  $\Omega$  yields the discretization in space and time,

$$\sum_{n=1}^N u_n(\tau + \delta) \int_{\Omega} a(\nabla u(\tau, x)) \varphi^n(x) \varphi^m(x) dx \\ + \int_{\Omega} b(x, \nabla u(\tau, x)) \nabla \varphi^n(x) \nabla \varphi^m(x) dx \\ = \int_{\Omega} c(x, u(\tau, x), \nabla u(\tau, x)) \varphi^m(x), \quad (3.1)$$

where

$$a(\xi) = \frac{1}{|\xi|}, \\ b(x, \xi) = \frac{\delta g(I_\sigma)(x)}{|\xi|}, \\ c(x, p, \xi) = \frac{p}{|\xi|} + \delta \gamma g(I_\sigma)(x).$$

Assuming that  $u(\tau)$  is known this is a system of linear equations for  $u_n(\tau + \delta)$ ,  $1 \leq n \leq N$ .

To avoid singular coefficients we regularize  $|\xi|$  in  $a$ ,  $b$  and  $c$  by replacing it by  $\Psi_\varepsilon(|\xi|)$ . In our case we chose  $\Psi_\varepsilon(|\xi|) = \sqrt{|\xi|^2 + \varepsilon^2}$ . Finally we get  $u(\tau + \delta)$  by approximating

$$u(\tau + \delta) \approx \sum_{n=1}^N u_n(\tau + \delta) \varphi^n,$$

where the  $u_n(\tau + \delta)$ ,  $1 \leq n \leq N$ , are the solutions of equation (3.1) with the  $\varepsilon$ -regularization in the coefficients mentioned above.

### 3.2 Spline evolution

Let  $\mathcal{C}_p^1([0, 1], \Omega)$  be the space of continuously differentiable and periodic curves equipped with the  $L^2$ -norm. Assume the basis of periodic cubic B-Splines  $\psi = (\psi^k : [0, 1] \rightarrow \mathbb{R})_{1 \leq k \leq K}$ ,  $\psi^k \in \mathcal{C}_p^1$  with uniformly distributed knots. Let further  $C(\tau)$  be a B-Spline curve based on  $(\psi^k)_{1 \leq k \leq K}$ . Thus, for  $\tau \geq 0$  we have

$$C(p(\tau)) = \sum_{k=1}^K p_k(\tau) \psi^k$$

where  $p(\tau) = (p_1(\tau), \dots, p_K(\tau))$ , and

$$p_k = (p_k^1, p_k^2) : [0, \infty[ \rightarrow \mathbb{R}^2, \quad 1 \leq k \leq K,$$

are the time-dependent spline control points. That is, we reinterpret the symbol  $C$  as a function which maps the spline control points  $p$  to a parametrized curve:

$$C : (\mathbb{R}^2)^K \rightarrow \mathcal{C}_p^1([0, 1], \mathbb{R}^2). \quad (3.2)$$

We denote the derivative of  $C(p)$  with respect to  $p$  as  $DC(p)$  and its adjoint as  $DC(p)^*$ . That means  $DC(p)$

linearly maps a  $v \in (\mathbb{R}^2)^K$  to  $DC(p)(v) \in \mathcal{C}_p^1([0, 1], \mathbb{R}^2)$ . Transforming the gradient descent in (2.3) to the evolution of the corresponding spline control points yields

$$DC(p)^* \circ DC(p) \circ \frac{\partial p}{\partial \tau} = -\nabla I(C(p)) \circ DC(p),$$

and consequently

$$\frac{\partial p}{\partial \tau} = -\nabla I(C(p)) \circ DC(p) \circ ((DC(p)^* \circ DC(p))^{-1}). \quad (3.3)$$

Let  $A$  be the matrix defined by

$$A_{ij} = \int_0^1 \psi^i(t) \psi^j(t) dt,$$

and  $B = A^{-1}$ . Then computation yields the explicit evolution of the  $i$ -th component of the  $k$ -th spline coefficient ( $i = 1, 2$  and  $1 \leq k \leq K$ ):

$$\frac{\partial p_k^i}{\partial \tau} = - \sum_{j=1}^K \int_{C(p)} (\nabla I(C(p))(t))^i \psi^j(t) B_{jk} dt. \quad (3.4)$$

We implemented (3.4) using explicit steps in time, i.e. we compute

$$p^i(\tau + \delta') = p^i(\tau) + \delta' \left( \int_{C(p)} \Phi(C(p))^i \psi^k ds \right) \circ (DC(p)^* \circ DC(p))^{-1}.$$

In our implementation we set  $\delta' = \delta/50$  for all examples.

### 3.3 Topology Adaptation

During the evolution of  $C(\tau)$  we adapt the spline curve to topology changes of level sets of  $u$ . After each step of the implicit evolution we look for self-intersections of every spline curve. As stated in the previous section we assume that the gradients of the level set function  $u(\tau)$  reflect the topology of the level sets. Thus, in case a self-intersection occurs, we check if  $\nabla u(\tau)/|\nabla u(\tau)|$  and the normals of the curve  $\mathbf{n}(\tau)$  locally coincide. If not, we split the curve into two and proceed with the evolution of  $k+1$  curves.

## 4 Electrical Impedance Tomography (EIT)

Assume a 2-dimensional, simply connected conductor  $\Omega$  with smooth boundary, a current flux  $f \in L^2(\partial\Omega)$ , and a closed curve  $\hat{C}$  in  $\Omega$ . Again denote the area inside and outside of  $\hat{C}$  as  $\mathcal{J}(\hat{C})$  and  $\mathcal{O}(\hat{C})$ , respectively. If the

conductivity is constantly 1 on  $\mathcal{O}(\hat{C})$  and 0 on  $\mathcal{J}(\hat{C})$ , then the electrical potential satisfies the following equation:

$$\begin{aligned} \Delta \varphi &= 0 & \text{on } \mathcal{O}(\hat{C}), \\ \frac{\partial \varphi}{\partial \mathbf{n}} &= f & \text{on } \partial\Omega, \\ \frac{\partial \varphi}{\partial \mathbf{n}} &= 0 & \text{on } \hat{C}. \end{aligned} \quad (4.1)$$

If the boundary  $\hat{C}$  is smooth, this problem has a unique weak solution in  $W^{1,2}(\mathcal{O}(\hat{C}))$  (e.g. [18, Section 3.6.]) We are concerned with the problem of obtaining the geometry of the inclusion from measurements of the electrical potential on the outside of the conductor, i.e. from  $\varphi|_{\hat{C}}$ . In [2] (see also [16]) the authors have shown that two measurements of  $\varphi|_{\hat{C}}$  (corresponding to two different current fluxes) are sufficient to reconstruct the inclusions.

Let  $u \in L^2(\Omega)$  and define the zero level set

$$\Omega_u := \overline{\{x \in \Omega : u(x) \leq 0\}}.$$

We introduce the *Neumann-to-Dirichlet* operator  $G_u : L^2(\partial\Omega) \rightarrow L^2(\partial\Omega)$ , which maps a current flux  $f$  to the trace of the solution of (4.1), where  $\hat{C}$  is replaced by  $\partial\Omega_u$  and  $\mathcal{O}(\hat{C})$  by  $\Omega_u$ . Now consider current fluxes  $f_i \in L^2(\partial\Omega)$  and electrical potentials  $g_i \in L^2(\partial\Omega)$  on the boundary of the conductor. We define the following Tychonov-type regularization functional (cf. [13])

$$F_\gamma(u) = \frac{1}{2} \sum_{i=1}^N \|G_u(f_i) - g_i\|_{L^2(\partial\Omega)}^2 + \frac{\gamma}{2} \|u\|_{L^2(\Omega)}^2. \quad (4.2)$$

Setting  $\varphi_i := G_u(f_i)$ , the formal derivative of  $F_\gamma$  with respect to  $\varphi$  is

$$\nabla F_\gamma(u) = - \sum_{i=1}^N \frac{\partial^2 \varphi_i}{\partial \mathbf{n}^2} \frac{v_i}{|\nabla u|} \delta_u + \gamma u, \quad (4.3)$$

where  $v_i$ ,  $1 \leq i \leq N$ , are the solutions of

$$\begin{aligned} \Delta v_i &= -(\varphi_i - g_i) & \text{on } \Omega \setminus \Omega_u, \\ \frac{\partial v_i}{\partial \mathbf{n}} &= 0 & \text{on } \partial\Omega \cup \partial\Omega_u, \end{aligned} \quad (4.4)$$

and  $\delta_u$  is the gradient of the indicator function of  $\Omega_u$  in the distributional sense, i.e. the 1-dimensional Dirac delta function along the zero level line of  $u$ . We propose the gradient flow

$$\frac{\partial u}{\partial \tau}(u(\tau)) = -\nabla F_\gamma(u(\tau)) \quad (4.5)$$

to minimize (4.2). For numerical implementations it is convenient to  $\varepsilon$ -regularize  $|\nabla u|$  in the denominator in (4.3) and to approximate  $\delta_u$  by a smooth kernel  $\delta_u^\varepsilon$ .

Again we propose a combined evolution of the level set functions and spline curves  $C_1, \dots, C_k$  similar to (2.4):

$$\begin{aligned} \frac{\partial u}{\partial \tau} &= -\nabla F_\gamma(u(\tau)), & u(0) &= u^0, \\ \frac{\partial C_j}{\partial \tau} &= -\nabla I(C_j(\tau)), & C_j(0) &= C_j^0, \end{aligned} \quad (4.6)$$

where for a curve  $C$

$$\begin{aligned} -\nabla I(C) &= \alpha \left( (u_2(C) - u \circ C)^2 \right. \\ &\quad \left. - (u_1(C) - u \circ C)^2 \right) |C'| \mathbf{n}_j \\ &\quad + \beta |C'| C''. \end{aligned}$$

As in Section 2 we denote by  $u_1(C)$  and  $u_2(C)$  the average value of the level set function  $u$  inside and outside the curve  $C$ , respectively. In addition to handling changes of the topology of the evolving curves (as in Section 3.3) the shape characteristics of the spline curves can be tracked. In case the inclusion  $\Gamma$  is a crack, i.e. a set of dimension 1, we can not detect it by the level set function  $u$  in the  $L^2$  sense anymore. The development of very thin curves  $C$  in the evolution (4.6) indicates such a case in advance.

Note that we are not able to prove that the level set function  $u$  converges to the indicator function of an inclusion  $\Gamma$  as we did in Theorem 1 for the case of image segmentation.

## 5 Results

In this section we present the numerical results for the combined evolution (2.4). In all test cases, except the ones shown in Figures 9 and 10, we chose  $\alpha = 10$ ,  $\beta = 0.1$  (with the exception of  $\beta = 3$  in the example in Figure 7) and the balloon force  $\gamma = 0.2$ . The time step  $\delta$  of the semi-implicit FE step varies from  $\delta = 20$  to  $\delta = 100$ . The number of steps of the implicit evolution is denoted by  $n$  in the illustrations, the number of steps of the explicit (curve) evolution is  $50n$ . With the exception of the first example we chose  $\varepsilon = 10^{-3}$  in the regularization of  $|\nabla u|^{-1}$ . The edge detection parameter is  $\eta = 100$ . In all the images the red curves are the spline curves corresponding to the  $C_j(\tau)$  in (2.4). The zero level set of the function  $u(\tau)$  is painted in green.

In Figure 5 we computed the combined evolution (2.4) for the cross presented in the introduction. To illustrate the influence of the regularization of  $|\nabla u|^{-1}$  we chose  $\varepsilon = 10^{-2}$  of one order larger. This example shows the stability of the spline curve compared to the zero level set of the geodesic active contour.

In Figure 6 we added salt & pepper noise to an underlying binary image. The spline curve adapts itself to the components of the object and attains a stable steady state. Figure 7 illustrates the regularizing effect

Implicit evolution	Combined evolution
$\approx 95$ seconds	$\approx 18$ seconds

**Table 1** Computation times.

of higher values for  $\beta$ . It also demonstrates that we detect high gradients and not areas of similar contrast. In Figure 8 we can observe the adaptation of the spline curve to the topology of the object by using the gradients of the level set function.

For illustrative reasons we chose different values of  $\delta$  in the above examples, but the evolutions behave the same, when setting  $\delta = 100$  and thus reducing the number of steps required to obtain the final image to  $n = 8$  and  $n = 10$  in Figure 5 and Figure 8 respectively.

In the last example the choice of parameters is different from above. We segmented cell clusters in DIC (Differential Interference Contrast) images. First we evolved the level set function without the spline curve and tried to choose the parameters such that the segmentation worked as well as possible (Figure 9). We then compared this result to the combined evolution with different parameters for the implicit part of the evolution (Figure 10). We observe that the results of both methods are roughly the same (the first one being more precise on the edges) but the combined evolution requires much less steps to reach the final segmentation. Considering the fact that the explicit evolution of the spline curves is fast compared to the implicit evolution this results in significantly lower computation times for the combined evolution (Table 1). In other words, the added curve evolution allows us to choose the parameters controlling the level set evolution such that the evolution is much faster than before without losing sensitivity. In addition, if we are mostly interested in the number of cell clusters, we can get this information immediately from the result of the combined evolution (simply by counting the number of spline curves).

**Acknowledgements** This work has been supported by the Austrian Science Foundation (FWF) Projects Y-123INF, FSP9202-N12, FSP9203-N12 and FSP9207-N12. We thank Jean-Paul Zolésio, INRIA, Sophia-Antipolis, France, for stimulating discussion. Finally we want to express our gratitude towards Heimo Wolinski, IMB-Graz, Karl-Franzens-Universität, Graz, Austria, and Bettina Heise, FLLL, Linz-Hagenberg, Austria, for the image data (Figures 9 and 10).

## References

1. G. Alessandrini. Stability for the crack determination problem. In L. Päiväranta and E. Somersalo, editors, *Inverse Problems in Mathematical Physics*, volume 422 of *LNP*, pages 1–8, 1993.
2. G. Alessandrini and A. Diaz Valenzuela. Unique determination of multiple cracks by two measurements. *SIAM J. Control Optim.*, 34:913–921, 1996.

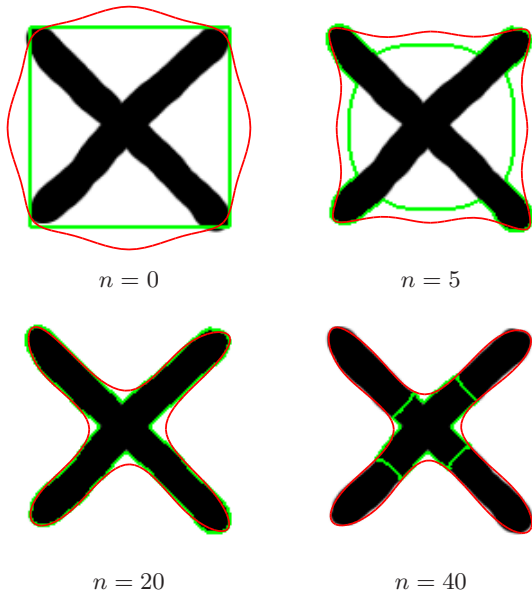


Fig. 5 Cross.  $\varepsilon = .01$ ,  $\delta = 20$ .

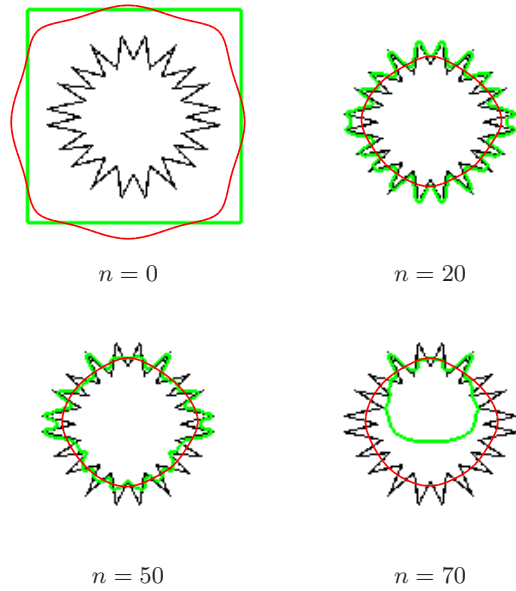


Fig. 7 Star-like object with large variation of the boundary.  $\beta = 3$ ,  $\delta = 100$ .

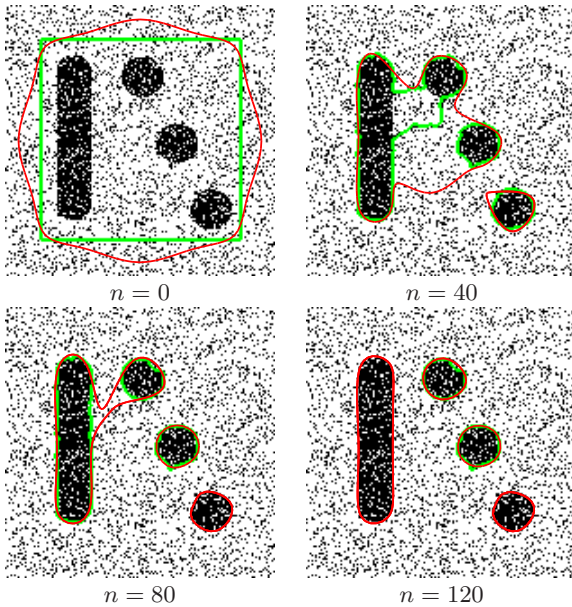


Fig. 6 Multiple segments with salt & pepper noise.  $\delta = 100$ .

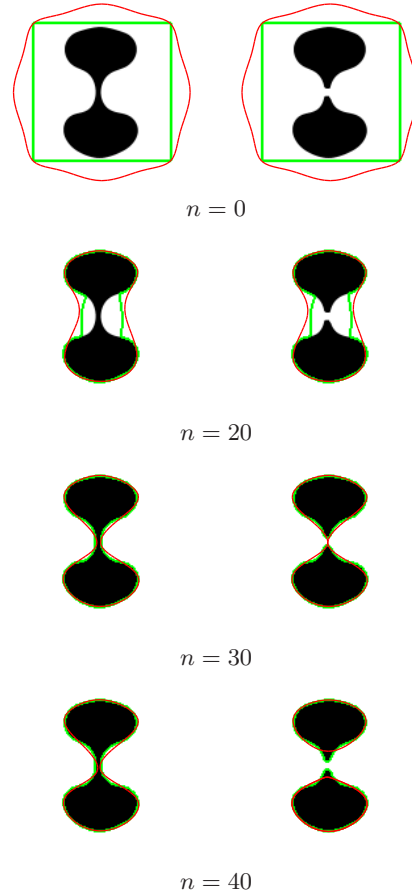
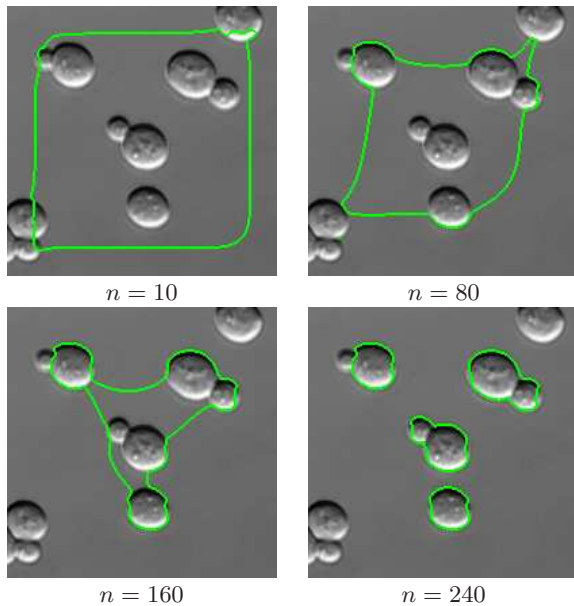
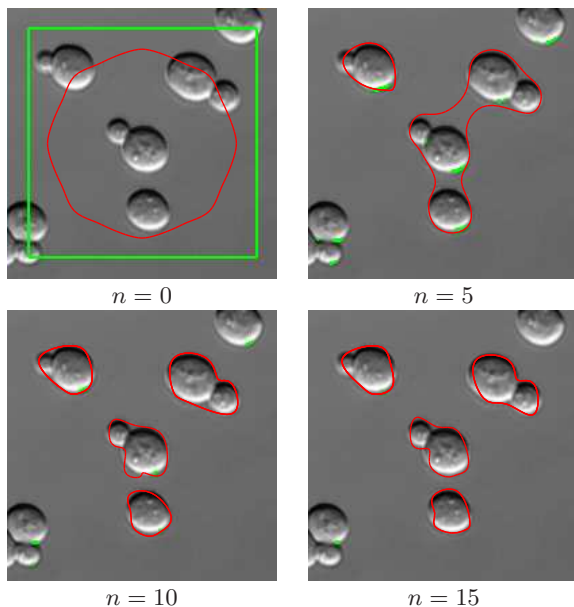


Fig. 8 Similar objects of different topology.  $\delta = 25$ .

3. Giovanni Alessandrini. Examples of instability of inverse boundary-value problems. *Inverse Problems*, 13(4):887–897, 1997.
4. Giovanni Alessandrini and Luca Rondi. Stable determination of a crack in a planar inhomogeneous conductor. *Inverse Problems*, 30(2):326–340, 1998.
5. Stéphane Andrieux, Amel Ben Abda, and Mohamed Jaoua. On the inverse emergent plane crack problem. *Mathematical Methods in the Applied Sciences*, 21:895–906, 1998.
6. Vicent Caselles, Francine Catté, and Françoise Dibos. A geometric model for active contours in image processing. *Numerische Mathematik*, 66:1–31, 1993.
7. Vicent Caselles, Ron Kimmel, and Guillermo Sapiro. Geodesic active contours. *International Journal of Com-*



**Fig. 9** Detection of cell clusters (active contours).  $\delta = 10$ ,  $\varepsilon = 0.001$ ,  $\gamma = 0.05$ ,  $\eta = 1000$ .



**Fig. 10** Detection of cell clusters (combined evolution).  $\delta = 100$ ,  $\varepsilon = 1.0$ ,  $\gamma = 0.5$ ,  $\eta = 1000$ .

- puter Vision*, 22(1):61–79, 1997.
8. Vicent Caselles, Ron Kimmel, Guillermo Sapiro, and Catalina Sbert. Minimal surfaces: A three dimensional segmentation approach. Technical Report 973, Technion EE Pub., 1995.
  9. Vicent Caselles, Ron Kimmel, Guillermo Sapiro, and Catalina Sbert. Minimal surfaces based object segmentation. *IEEE Transactions on Pattern Analysis and Machine Intelligence*, 19(4):394–398, 1997.
  10. Tony F. Chan and Xue-Cheng Tai. Level set and total variation regularization for elliptic inverse problems with discontinuous coefficients. *Journal of Computa-*

*tional Physics*, 193(1):40–66, 2004.

11. Tony F. Chan and Luminita A. Vese. Active contours without edges. *IEEE Transactions on Image Processing*, 10(2):266–277, 2001.
12. Eric T. Chung, Tony F. Chan, and Xue-Cheng Tai. Electrical impedance tomography using level set representation and total variational regularization. *Journal of Computational Physics*, 205(1):357–372, 2005.
13. Heinz W. Engl, Martin Hanke, and Andreas Neubauer. *Regularization of Inverse Problems*, volume 375 of *Mathematics and Its Applications*. Kluwer Academic Publishers, Dordrecht Boston London, 2000.
14. Avner Friedman and Michael Vogelius. Determining cracks by boundary measurements. *Indiana Univ. Math. J.*, 38:527–556, 1989.
15. M. Kass, A. Witkin, and D. Terzopoulos. Snakes active contour models. *International Journal of Computer Vision*, 1(4):321–331, 1988.
16. Hyunseok Kim and Jin Keun Seo. Unique determination of a collection of a finite number of cracks from two boundary measurements. *SIAM J. Math. Anal.*, 27:1336–1340, 1996.
17. Gerald Kühne, Joachim Weickert, Markus Beier, and Wolfgang Effelsberg. Fast implicit active contour models. In *Pattern Recognition : 24th DAGM Symposium, Zurich, Switzerland, September 16-18, 2002. Proceedings*, volume 2449 of *Lecture Notes in Computer Science*, pages 133–140, Berlin/Heidelberg, 2002. Springer.
18. Olga A. Ladyshenskaya and Nina N. Ural'tseva. *Linear and Quasilinear Elliptic Equations*, volume 46 of *Mathematics in Science and Engineering*. Academic Press, New York and London, 1968.
19. D. Mumford and J. Shah. Boundary detection by minimizing functionals. In *Proc. IEEE Conf. Computer Vision Pattern Recognition*, pages 22–26, 1985.
20. D. Mumford and J. Shah. Optimal approximations by piecewise smooth functions and associated variational problems. *Commun. Pure Appl. Math.*, 42(4):577–684, 1989.
21. S. Osher and J.A. Sethian. Fronts propagating with curvature-dependent speed: Algorithms based on hamilton–jacobi formulations. *Journal of Computational Physics*, 79:12–49, 1988.
22. Huaiping Yang, Matthias Fuchs, Bert Jüttler, and Otmar Scherzer. Evolution of t-spline level sets with distance field constraints for geometry reconstruction and image segmentation. In *IEEE International Conference on Shape Modeling and Applications 2006 (SMI'06)*, pages 247–252, Los Alamitos, CA, USA, 2006. IEEE Computer Society.